International Journal of Nanomedicine

Dovepress

open access to scientific and medical research

Open Access Full Text Article

ORIGINAL RESEARCH

Microdroplets Encapsulated with NFATc1-siRNA and Exosomes-Derived from MSCs Onto 3D Porous PLA Scaffold for Regulating Osteoclastogenesis and Promoting Osteogenesis

Peng Luo[1,*], Yi Zhang[2,3,*], Maodi Huang[1], Guochen Luo[1], Yaping Ma[1,4], Xin Wang[1,4]

[1]Department of Orthopaedic Surgery, Affiliated Hospital of Zunyi Medical University, Zunyi, Guizhou, 563003, People's Republic of China; [2]Department of Hygiene Toxicology, School of Public Health, Zunyi Medical University, Zunyi, Guizhou, 563000, People's Republic of China; [3]Key Laboratory of Maternal & Child Health and Exposure Science of Guizhou Higher Education Institutes, Zunyi Medical University, Zunyi, Guizhou, 563000, People's Republic of China; [4]Guizhou Provincial Key Laboratory of Medicinal Biotechnology in Colleges and Universities, Zunyi Medical University, Zunyi, Guizhou, 563000, People's Republic of China

*These authors contributed equally to this work

Correspondence: Xin Wang, Department of Orthopaedic Surgery, Affiliated Hospital of Zunyi Medical University, Zunyi, Guizhou, 563003, People's Republic of China, Tel +86 136 3928 8558, Fax +86-851-2860 8903, Email xin.wang@zmu.edu.cn

Introduction: Osteoporotic-related fractures remains a significant public health concern, thus imposing substantial burdens on our society. Excessive activation of osteoclastic activity is one of the main contributing factors for osteoporosis-related fractures. While polylactic acid (PLA) is frequently employed as a biodegradable scaffold in tissue engineering, it lacks sufficient biological activity. Microdroplets (MDs) have been explored as an ultrasound-responsive drug delivery method, and mesenchymal stem cell (MSC)-derived exosomes have shown therapeutic effects in diverse preclinical investigations. Thus, this study aimed to develop a novel bioactive hybrid PLA scaffold by integrating MDs-NFATc1-silencing siRNA to target osteoclast formation and MSCs-exosomes (MSC-Exo) to influence osteogenic differentiation (MDs-NFATc1/PLA-Exo).

Methods: Human bone marrow-derived mesenchymal stromal cells (hBMSCs) were used for exosome isolation. Transmission electron microscopy (TEM) and confocal laser scanning microscopy were used for exosome and MDs morphological characterization, respectively. The MDs-NFATc1/PLA-Exo scaffold was fabricated through poly(dopamine) and fibrin gel coating. Biocompatibility was assessed using RAW 264.7 macrophages and hBMSCs. Osteoclast formations were examined via TRAP staining. Osteogenic differentiation of hBMSCs and cytokine expression modulation were also investigated.

Results: MSC-Exo exhibited a cup-shaped structure and effective internalization into cells, while MDs displayed a spherical morphology with a well-defined core-shell structure. Following ultrasound stimulation, the internalization study demonstrated efficient delivery of bioactive MDs into recipient cells. Biocompatibility studies indicated no cytotoxicity of MDs-NFATc1/PLA-Exo scaffolds in RAW 264.7 macrophages and hBMSCs. Both MDs-NFATc1/PLA and MDs-NFATc1/PLA-Exo treatments significantly reduced osteoclast differentiation and formation. In addition, our results further indicated MDs-NFATc1/PLA-Exo scaffold significantly enhanced osteogenic differentiation of hBMSCs and modulated cytokine expression.

Discussion: These findings suggest that the bioactive MDs-NFATc1/PLA-Exo scaffold holds promise as an innovative structure for bone tissue regeneration. By specifically targeting osteoclast formation and promoting osteogenic differentiation, this hybrid scaffold may address key challenges in osteoporosis-related fractures.

Keywords: bioactive microdroplets, PLA scaffold, MSC-Exo, biocompatibility, osteoclast formation, hBMSCs, osteogenesis

Received: 24 November 2023
Accepted: 1 April 2024
Published: 9 April 2024

Graphical Abstract

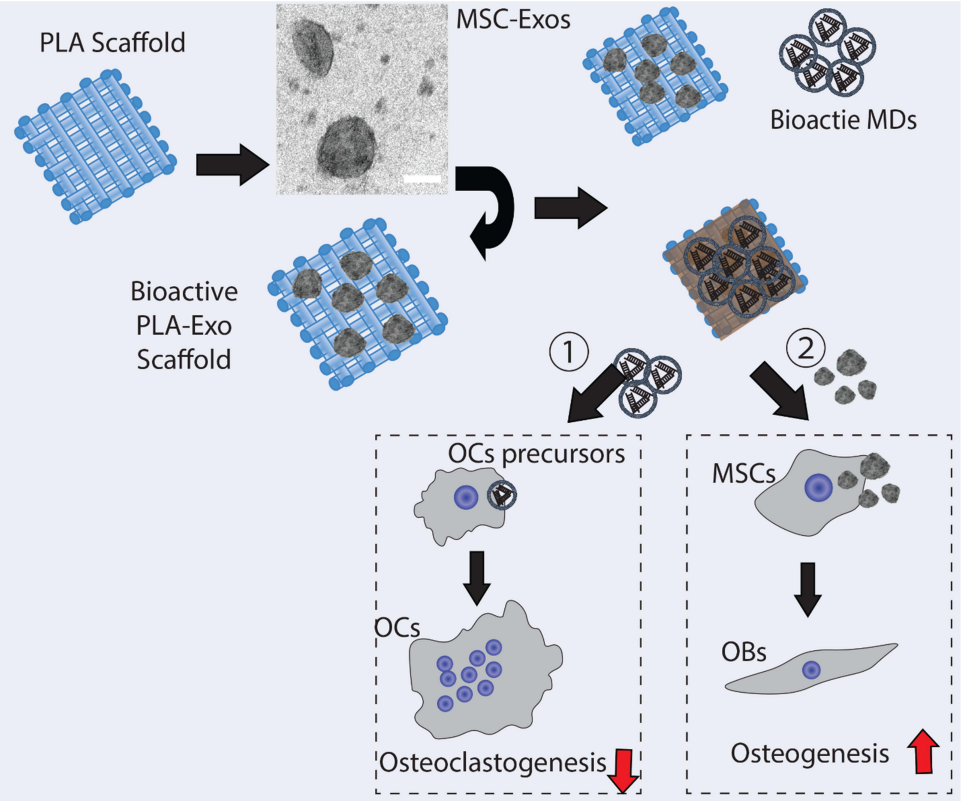

Introduction

Osteoporosis and Its Burdens

Osteoporosis stands as one of the prevalent bone diseases characterized by the deterioration of bone tissue structure and a decline in bone density, particularly prevalent in the aging population.[1] As a result, increased bone fragility and fracture risk, especially in hip, spine, hip, wrist, and pelvis, etc. were frequently recorded in osteoporotic patients.[2] Furthermore, studies also indicated that female patients over the age of 50 years are more likely to develop osteoporosis than their male counterparts.[3] In the United States alone, it is estimated that there are over 10 million individuals with osteoporosis and osteoporosis-induced fractures. Additionally, approximately 34 million Americans are considered at risk of developing osteoporosis.[4] Globally, more than 200 million women are affected by osteoporosis.[5]

Osteoporotic Fracture Treatment

The continuous renewal of bone, known as bone remodeling, is achieved through the coordinated activities of osteoblastic bone formation and osteoclastic bone resorption.[6] The harmonious equilibrium between osteoblastic bone formation and osteoclast-mediated bone resorption is crucial for preserving bone density, ensuring homeostasis, and facilitating the repair of fractures and damaged bone tissues.[7] In diverse pathological circumstances, the heightened activation of osteoclasts leads to resorptive bone disorders such as osteoporosis, rheumatoid arthritis, periprosthetic osteolysis, Paget's disease, etc.[8] Currently, various antiresorptive agents (bisphosphonate) or RANKL binding antibody, are commonly used in the treatment of osteoclast overactivation, thereby diminishing resorption of bone.[9,10] However, some sever adverse events, especially long-term use of bisphosphonate, were reported in several epidemiologic studies.[11] Presently, several therapeutic options were used to treat osteoporotic fracture, including surgical immobilization of the fracture, application of antiresorptive therapy, and using various synthetic and naturally occurring bone grafts to repair

osteoporotic fractures.[12,13] Various tissue engineered scaffolds were fabricated and served as structural support for cell attachment and differentiation.[14]

PLA Scaffold and Its Limitations

Polylactic acid (PLA) is a synthetic polyester extensively employed in orthopedic engineering for treating bone defects, attributed to its versatile fabrication, biodegradability, and compatibility.[15] In addition, PLA scaffold or formulation containing PLA have also been approved by the US Food and Drug Administration (FDA) for clinical usage and direct contact with biological fluids.[16] Previous studies also indicated that the porosity and pore size of 3D printed PLA scaffold are crucial for its biological functionality, including cell attachment, migration, and bone regeneration.[17] However, PLA-based scaffolds are relatively bioinert, thereby demanding certain modification with bioactive molecules, growth factors, osteoinductive molecules, and living cells to increase their bio-functionality.

Exosomes and Its Applications in Regenerative Medicine

Exosomes are nanosized membrane vehicles (30–150 nm) secreted by almost all types of cells.[18] It has been demonstrated that exosomes play an important role in intercellular communication via delivering various effectors or signaling molecules from parents' cells to recipient cells.[19] Exosomes derived from mesenchymal stem cells (MSCs) have been demonstrated as vital components to contribute tissue regeneration similar to their parent cells[20] under various physiological and pathological conditions. MSCs-exosomes have been shown to repair damaged bone[21] and cartilage,[22] acute liver failure,[23] myocardial infarction after ischemic injury,[24] and renal injury,[25] etc. Hence, MSCs-derived exosomes have arisen as a promising therapeutic strategy for targeted tissue regeneration.

Fabrication of Dual Bio-Functional PLA Scaffolds

Ultrasound is one of the most widely used diagnostic and treatment methods in clinics due to its non-invasive procedure.[26] Additionally, ultrasound, including low frequency (< 100kHz) and high frequency (> 100kHz), has been considered as one of the promising delivery systems for gene and drug delivery.[27] Microdroplets (MDs) are small spherical carriers consisting of a gas core, which have been used as ultrasonic contrast agent in the medical imaging and drug delivery systems[28,29]. For example, Yin et al have developed ultrasound-responsive siRNA-encapsulated nanobubbles for glioma treatment. Their results showed significantly increased gene delivery efficiency in vitro and in vivo[30]. Binding of receptor activator of nuclear factor kappa-B (RANK) and its ligand RANKL are essential for osteoclast development and activation.[31] Following RANK-RANKL interaction, several cytoplasmic adaptor proteins and downstream signaling pathways were activated,[32] including the nuclear factor of activated T cells cytoplasmic 1 (NFATc1), which serve as a master regulator for osteoclast differentiation[33] and the expression of osteoclastic genes.[34] Therefore, in this study, we intend to develop a dual bio-functional PLA scaffolds to regulate osteoclast differentiation and formation via MDs-guided NFATc1 delivery system and an additional exosome-based modification strategy to increase osteogenesis. Our results indicate that this novel MDs-NFATc1/PLA-Exo scaffold may serve as a potential therapeutic scaffold for hard tissue regeneration.

Materials and Methods

Cell Culture and Exosome Purification

For exosome isolation, human bone marrow-derived mesenchymal stromal cells (hBMSCs, ATCC® PCS-500-012™) were used in this study. The cells were cultured in Dulbecco's Modified Eagle's Medium (DMEM; Life Technologies Pty Ltd., China) supplemented with 10% fetal bovine serum (FBS; Biological Industries, LTD, Beit Haemek, Israel), and 1% (v/v) penicillin/streptomycin (Solarbio, Beijing, China) in a 5% CO_2 atmosphere at 37 °C. To collect conditioned medium (CM), hBMSCs at passage 3 were seeded in T75 flasks and cultured until reaching 90% confluence at 37 °C. After triple rinsing with phosphate-buffered saline (PBS), the cells were cultured with 10 mL DMEM supplemented with 10% exosome-depleted FBS at 37 °C for 24 h before CM collection. The gathered CM was combined for exosome isolation. Initially, CM was filtered through 0.22 μm filters to eliminate live cells and other large membranous structures.

Subsequently, CM underwent centrifugation at 300×*g* at 4 °C for 10 min, followed by transfer to new tubes and centrifugation at 2000×g at 4 °C for 20 min. Next, the CM was centrifuged in a 45Ti rotor (Beckman) at 10,000×g at 4 °C for 40 min. The supernatant was then spun at 100,000×g at 4 °C for 90 min to pellet exosomes. The resulting exosome pellets were resuspended in PBS, aliquoted, and promptly stored at −80 °C.

Transmission Electron Microscopy (TEM)

Exosomes (5 μL) were deposited onto 200 mesh TEM copper grids coated with formvar carbon film for 5 min at room temperature. Subsequently, they were stained with 1% uranyl acetate for 15–20 s. Any surplus uranyl acetate was eliminated by rinsing with deionized water three times. The samples were dried using Whatman filter paper before imaging. A JEM-1400, JOEL TEM operated at a voltage of 80 kV was utilized to capture images of the exosome samples.

Exosome Labeling and Cellular Uptake of Exosomes

Exosome labeling was carried out using the PKH67 green fluorescent cell linker kit for general cell membrane labeling, following the manufacturer's instructions (PKH67GL-1KT, Sigma, China). In summary, PKH67-labeled exosomes were incubated with recipient cells at 37 °C for the specified time points. Post-treatment, cells underwent three washes with PBS, were fixed using 4% paraformaldehyde, permeabilized with 0.25% Triton, and then stained with Alexa Fluor 594-labeled phalloidin for 1 h, followed by DAPI staining. Images were acquired using a confocal laser scanning microscope with a × 40 objective (Leica DM IRB; Leica, Wetzlar, Germany).

Fabrication of MDs-NFATc1/PLA-Exo Hybrid Scaffold

The creation of Bovine Serum Albumin (BSA)-stabilized bioactive MDs-NFATc1 followed established procedures from previous studies.[35,36] In summary, a mixture of 50 nM NFATc1 siRNA (sc-29,412, Santa Cruz Biotechnology), 300 μL perfluorocarbon, 4 mL of PBS, and 40 mg of BSA (Sigma Aldrich, China) underwent sonication for the fabrication of MDs-NFATc1. Ultracentrifugation was then conducted using the Beckman Coulter Optima XPN-100 ultracentrifuge, spinning for 30 minutes at 14,000 rpm. For fluorescence imaging, fluorescein isothiocyanate (FITC)-labeled BSA (Sigma, China) was employed in the MDs-NFATc1 fabrication. The ultrasound stimulation of MDs-NFATc1 was performed following the established protocol in our previous study.[37] In summary, FITC-labeled MDs-NFATc1 were first diluted into PBS. Subsequently, they were exposed to ultrasound stimulation utilizing a portable home use ultrasound pain therapy device, which operated at an acoustic frequency of 1 MHz and a power of 1 W/cm^2 for a duration of 10 minutes (MYCHWAY, China). Following ultrasound treatment, the MDs-NFATc1 were transferred into a Glass Bottom Confocal Dish for imaging. The images were captured using a confocal laser scanning microscope equipped with a ×40 objective lens (Leica DM IRB; Leica, Wetzlar, Germany).

3D-printed PLA scaffolds were generated using a custom 3D printer in accordance with our prior study.[38] Briefly, PLA filament with a diameter of 1.75 mm was directly supplied to the printer head and extruded through the printing nozzle at a temperature of 210 °C. The resulting scaffolds were printed with dimensions of 10 mm in diameter and 4 mm in height. Surface modification through a poly(dopamine)-based approach and functionalization with exosomes followed methods detailed in our previous work.[38] To elaborate, a poly(dopamine) (PDA) coating on PLA scaffolds was achieved by utilizing 4 mg/mL dopamine hydrochloride in a 10 mM pH = 8.5 Tris buffer for 1 h with continuous stirring, followed by rinsing with deionized water. The fabrication of exosome-functionalized PLA scaffolds (PLA-Exo) was performed according to our previous study.[38] Briefly, exosomes (10 μg in terms of protein) were incubated with PDA-modified PLA scaffold for 1 h at room temperature. For fluorescence imaging, PKH67-labeled exosomes were employed for PLA scaffold modification, and images were captured using a confocal laser scanning microscope with a ×40 objective (Leica DM IRB; Leica, Wetzlar, Germany).

Preparation of the fibrin gel was conducted in line with a previous study, with minor adjustments.[39] In brief, 20 mg of MDs-NFTAc1 was diluted in PBS and subjected to ultrasound exposure with an acoustic frequency of 1 MHz using a portable home use ultrasound pain therapy device for 10 min (MYCHWAY, China). Subsequently, 40 μL of thrombin was added to the MDs-NFTAc1 solution, reaching a final thrombin concentration of 4 U/mL. The resulting solution was

evenly mixed with fibrinogen solution (10 mg/mL in PBS) and incubated with the PLA-Exo scaffold for 10 to 15 min, resulting in the formation of the MDs-NFATc1/PLA-Exo hybrid scaffold. For fluorescence imaging, FITC-labelled MDs was used for scaffold fabrication with the same methods mentioned above. Images were captured using a confocal laser scanning microscope with a ×40 objective (Leica DM IRB; Leica, Wetzlar, Germany).

Biocompatibility Assay in RAW264.7 Macrophages and hBMSCs

The MTT cell proliferation assay served as an indicator of metabolic activity for assessing cell viability. Cells were initially seeded on tissue culture-treated cover slips overnight, followed by rinsing with PBS and co-culturing with different scaffolds. On both day 1 and day 3, 5 mg/mL of 3-(4,5-dimethylthiazol-2-yl)-2,5-diphenyl tetrazolium bromide (MTT, Sigma, China) was introduced to the wells and allowed to incubate for an additional 4 h at 37 °C. Subsequently, dimethyl sulfoxide (DMSO) was utilized to dissolve the formazan generated during the incubation period. The absorbance of the sample was then measured using a microplate reader at 570 nm.

Live/dead staining was performed using the Calcein/PI live/dead viability assay kit, following the guidelines provided by the manufacturer (Beyotime, China). Cells were subjected to incubation with the staining solution at room temperature on both day 1 and day 3. Subsequent to washing with PBS, the samples were examined using a confocal laser scanning microscope with a × 10 objective (Leica, Wetzlar, Germany).

MDs-NFATc1 Release and Internalization Study

The release and internalization of MDs-NFATc1 into cells were assessed through confocal laser scanning microscopy. In brief, FITC-labeled MDs-NFATc1 were utilized for scaffold modification. Cells were seeded on tissue culture-treated coverslips overnight and subsequently co-cultured with the MDs-NFATc1/PLA-Exo hybrid scaffold at 37 °C. Following PBS washing, the cells were fixed with 4% paraformaldehyde, permeabilized using 0.25% Triton, and stained with Alexa Fluor 594-labeled phalloidin for 1 h, followed by DAPI staining. Images were captured using a confocal laser scanning microscope with a × 40 objective (Leica DM IRB; Leica, Wetzlar, Germany).

Exosome Release and Internalization Study

The exosome internalization assay was conducted following the method from our previous study[38]. In brief, the PKH67 cell membrane labeling kit was employed to label exosomes for modification of the PLA scaffold. Cells were initially seeded on tissue culture-treated coverslips overnight, followed by co-culturing with the MDs-NFATc1/PLA-Exo hybrid scaffold for the specified time points at 37 °C. After PBS washing, the cells were fixed with 4% paraformaldehyde, permeabilized using 0.25% Triton, and subjected to staining with Alexa Fluor 594-labeled phalloidin for 1 h, followed by DAPI staining. Subsequent imaging was performed using a confocal laser scanning microscope with a × 40 objective (Leica DM IRB; Leica, Wetzlar, Germany).

Tartrate-Resistant Acid Phosphatase (TRAP) Staining

Human osteoclast precursors (2T-110) were obtained from Lonza, China. These precursors were cultured in the presence of various scaffolds using osteoclast precursor growth medium (Lonza, China). The medium was supplemented with 1% (v/v) penicillin/streptomycin, 10% FBS, 2 mM L-glutamine, M-CSF, and RANKL. TRAP staining was performed according to the established protocols.[40] After staining, osteoclast cells were identified as multinucleated, TRAP-positive cells with three or more nuclei. The images of the stained sections were captured using an inverted microscope with a ×20 objective (Leica, Wetzlar, Germany).

The Effect of MDs-NFATc/PLA-Exo Hybrid Scaffold on hBMSCs Osteogenic Differentiation

For osteogenic differentiation, hBMSCs were plated on culture coverslips and allowed to reach confluence. Subsequently, the cells underwent three washes with PBS and were co-cultured with various scaffolds in osteogenic differentiation

medium (DMEM supplemented with 10% FBS, 1% penicillin/streptomycin, and 10 mM β-glycerophosphate, 50 mM L-ascorbic acid 2-phosphate, 100 nM dexamethasone). The culture medium was refreshed every three days.

Immunofluorescence Staining for Osteogenic-Related Markers

Immunofluorescent staining was employed to assess the expression of osteogenic-related markers (ALP and OCN). In brief, cells were rinsed with PBS, fixed in 4% paraformaldehyde, permeabilized using 0.25% Triton X-100, blocked with 4% bovine serum albumin (BSA), and then incubated overnight at 4°C with rabbit polyclonal antibodies to ALP (1:100, ab224335, Abcam) or anti-osteocalcin antibody (1:100, Santa Cruz Biotechnology). Fluorescein isothiocyanate-conjugated goat anti-rabbit IgG (H+L) was used as the secondary antibody. Subsequently, samples were mounted with ProLong™ Gold Antifade Mountant with DAPI (P36935, Thermo Fisher Scientific, China), and images were acquired using a confocal laser scanning microscope with a ×20 objective (Leica DM IRB; Leica, Wetzlar, Germany).

Alkaline Phosphatase (ALP) Staining

To evaluate osteogenic differentiation in hBMSCs, ALP staining was conducted at 14 days using the BCIP/NBT Alkaline Phosphatase Color Development Kit following the manufacturer's instructions (Beyotime, Shanghai, China). The presence of purple deposits indicated areas with high ALP activity. Images were captured using an inverted light microscope with a ×10 objective (Leica, Wetzlar, Germany).

Alizarin Red S Staining

On the 21st day of culture, the specimens were collected for Alizarin Red S staining to assess mineralization of hBMSCs. In brief, cells were fixed with 4% paraformaldehyde, rinsed with deionized water, and stained with a 2% Alizarin Red S staining solution (pH = 4.1) for 20 min at room temperature. Following thorough washing with deionized water, the plates were left to air-dry overnight. Images were captured using an inverted light microscope with a ×10 objective (Leica, Wetzlar, Germany). Quantification of Alizarin Red S staining was performed according to the previous study.[41]

Osteogenic-Related Gene Expression Analysis by Reverse Transcription-Quantitative PCR (RT-qPCR)

To assess the impact of various scaffolds on the osteogenic differentiation of hBMSCs, total RNA was isolated from hBMSCs at 14 days using TRIzol reagent (15,596,026; Thermo Fisher Scientific, China) following the manufacturer's guidelines.The purity and concentration of RNA were evaluated using a NanoDrop spectrophotometer (NanoDrop technologies). Subsequently, cDNA was synthesized from 500 ng of total RNA using a RevertAid First Strand cDNA Synthesis Kit (K1622, Thermo Fisher Scientific, China). Quantification of osteogenic-related gene expression was conducted through RT-PCR using SYBR Green qPCR Master Mix (Life Technologies, China) on the QuantStudio Real-Time PCR system. The relative gene expression was calculated using the comparative Ct ($2^{-\Delta\Delta CT}$) method.[42]

Cytokine Antibody Array

The Human XL cytokine array (Proteome Profiler Human XL cytokine arrays, ARY022, R&D Systems) was conducted following the manufacturer's instructions. Briefly, hBMSCs were co-cultured with either MDs-NFATc1/PLA scaffold or MDs-NFATc1/PLA-Exo hybrid scaffold for 3 days in osteogenic medium. Membranes were exposed to the collected supernatant overnight at 4°C. After thorough washing, the membranes were incubated with a detection antibody cocktail for 1 h at room temperature and treated with streptavidin-horseradish peroxidase (HRP) solution for 30 min. The resulting signal was visualized using an enhanced chemiluminescence detection system and exposed to X-ray films. Subsequently, images were captured and semi-quantified in the ImageJ software to determine the integrated density value of each protein spot on the grayscale.

Statistical Analysis

The data were presented as mean ± standard deviations (SD, $n = 3$). Statistical analysis was conducted using GraphPad Prism 7 (Version 7.02) for Windows (GraphPad Software Inc., USA). Group differences were assessed through one-way

analysis of variance (ANOVA) with Bonferroni's multiple comparison tests. A p-value of less than 0.05 was considered statistically significant.

Results

Purification and Characterization of Exosomes Isolated from hBMSCs

To validate successful exosome isolation, transmission electron microscopy was used for morphological characterization. Figure 1A displays the morphology of exosomes isolated from hBMSCs, revealing spherical or cup-shaped structures. To examine the internalization of exosomes into recipient cells, exosomes were labeled with the green fluorescent marker PKH67 and then incubated with RAW264.7 macrophages and hBMSCs. Figure 1B clearly illustrates the uptake of exosomes by RAW 264.7 macrophages, as indicated by the presence of green punctate around the perinuclear region. As depicted in Figure 1C, internalization of exosomes into hBMSCs was evident at 6 hours post-stimulation, while a similar increase of accumulated exosome levels in hBMSCs was found at 24 h post-stimulation. In addition, mean fluorescence intensity at 24 h post-incubation shows a significant increase compared to fluorescence intensity at 6 h (Figure 1C).

Fabrication of MDs-NFATc1/PLA-Exo Hybrid Scaffold

The morphology of the MDs-NFATc1 is presented in Figure 2A. Confocal laser scanning microscopy images demonstrated spherical morphology of MDs-NFATc1 with a well-defined core-shell structure. The core-shell structure appeared

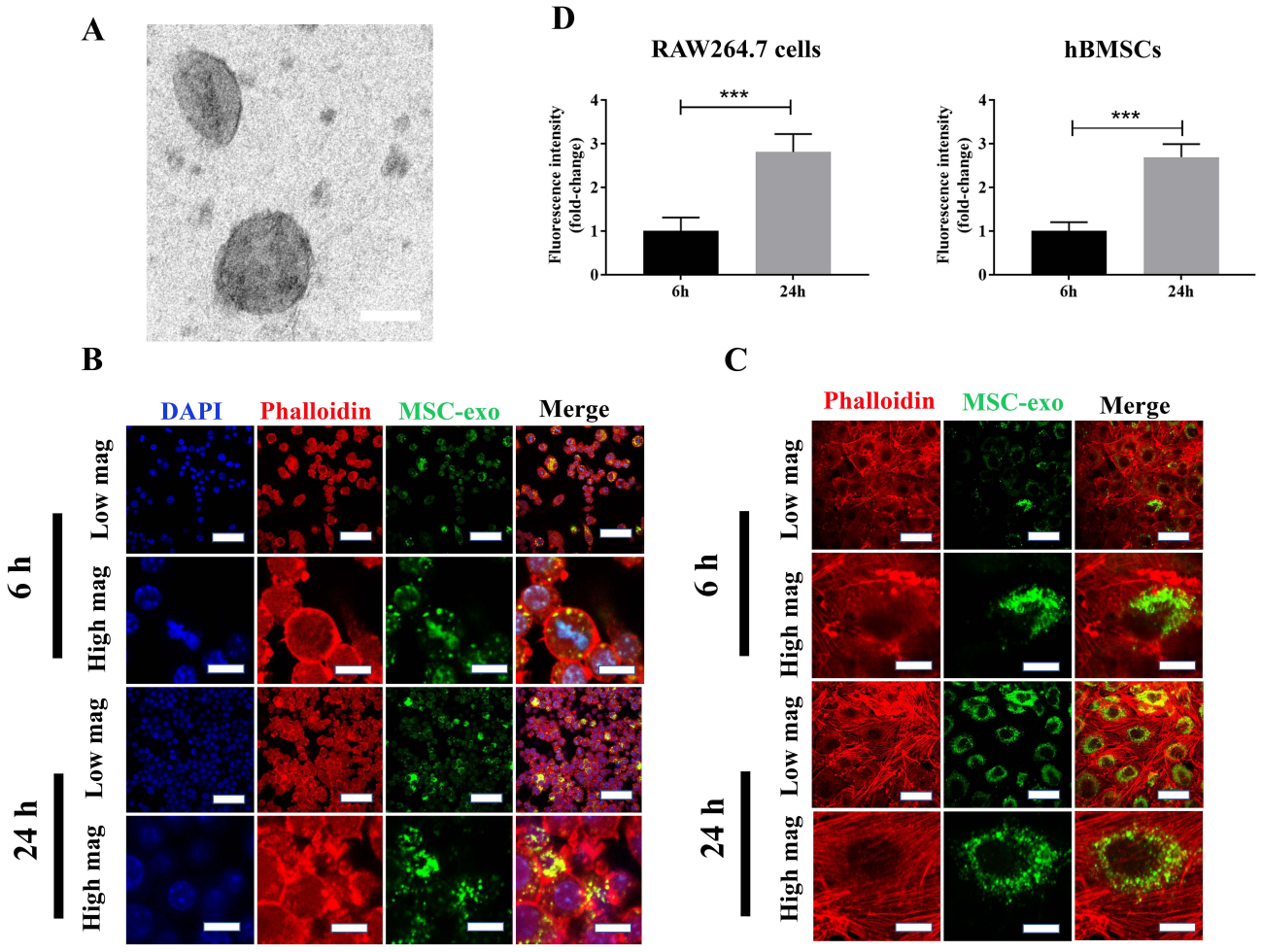

Figure 1 Characterization of hBMSCs-derived exosomes. (**A**) Morphological characterization of MSCs-Exosome via TEM. MSCs-Exosome exhibited cup-shaped morphology. Scale bar = 80 nm. (**B**) Internalization of PKH26-labeled MSCs-Exo into RAW264.7 cells. PKH67-labeled MSCs-exosome exhibit red color, while actin filament and nuclei were stained with red and blue color, respectively. (**C**) Internalization of PKH67-labeled MSCs-Exo into hBMSCs. Intracellular PKH67-labeled MSCs-exosomes were detected around peri-nuclei areas in hBMSCs by confocal laser scanning microscopy. Nuclei were stained with DAPI (blue) and F-actin filaments were stained with phalloidin (red). Scale bar = 50 μm (low mag), Scale bar = 10 μm (high mag). (**D**) Quantification of fluorescence intensity. Significant difference: ***$p < 0.001$.

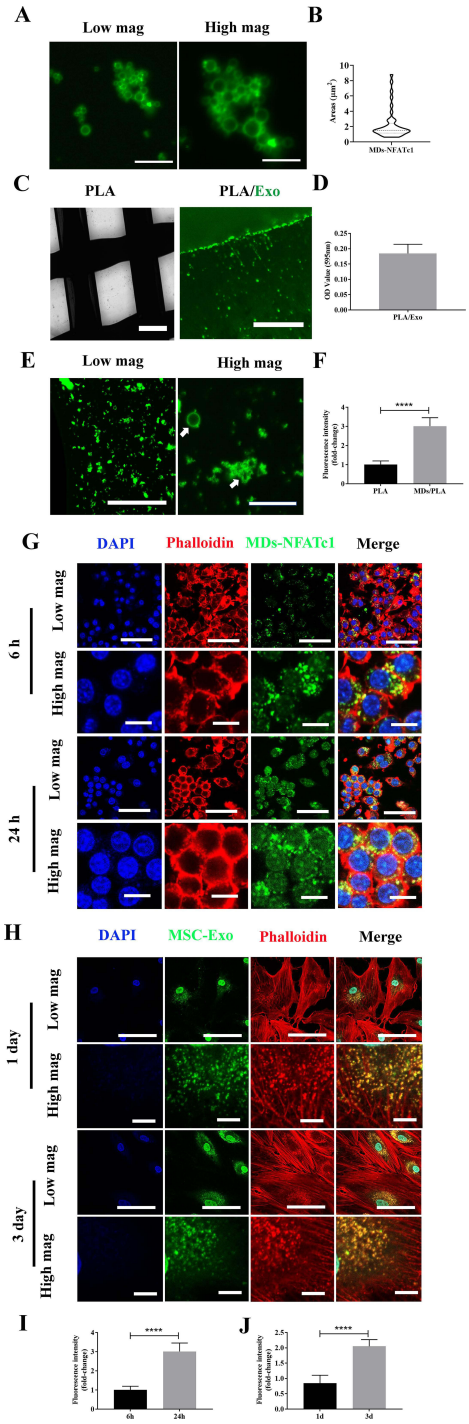

Figure 2 Fabrication of MDs-NFATc1/PLA-Exo hybrid scaffold (**A** and B) Representative confocal laser scanning microscopy images showing formation of MDs-NFATc1 and quantification of areas. Images were captured using a confocal laser scanning microscopy. Scale bar = 10 μm (left), Scale bar = 5 μm (right). (**C** and **D**) Representative phase contrast image for the 3D printed PLA scaffold and confocal laser scanning microscopy image showing PLA scaffold functionalized with PKH67-labeled exosomes and protein quantification. Scale bar = 500 μm (left), Scale bar = 20 μm (right). (**E** and **F**) Representative confocal laser scanning microscopy images showing the functionalization of MDs-NFATc1 on PLA/Exo scaffold and quantification of MDs-NFATc1intensity. Scale bar = 100 μm (left), Scale bar = 20 μm (right). (**G**) Representative confocal laser scanning microscopy images showing the uptake of FITC-labeled MDs released from MDs-NFATc1/PLA-Exo hybrid scaffold into RAW 264.7 macrophages. The actin filaments were stained in red color, while the cell nuclei were stained in blue. Scale bar = 50 μm (low magnification), Scale bar = 10 μm (high magnification). (**H**) Representative confocal laser scanning microscopy images showing the uptake of MSC-exosomes released from MDs-NFATc1/PLA-exosome scaffold into hBMSCs at 1 day and 3 days. Exosomes were prelabeled with PKH67. Scale bar = 100 μm (low magnification), Scale bar = 10 μm (high magnification). (**I**) The fluorescence intensity of FITC-labeled MDs released from the MDs-NFATc1/PLA-Exo hybrid scaffold was quantified. (**J**) Quantification of fluorescence intensity of MSC-exosomes released from MDs-NFATc1/PLA-exosome scaffold. Significant difference: ****$p < 0.0001$.

to be consistent across all the samples, indicating homogeneous composition and distribution. The quantitative analysis of MDs-NFATc1 areas revealed an average area of 2.2 μm² (Figure 2B).

Figure 2C shows a phase contrast image of a 3D printed PLA scaffold's macroscopic structure and architecture. Furthermore, confocal laser scanning microscopy images demonstrates the functionalization of the 3D printed PLA scaffold with MSC-Exo. The successful integration of exosomes onto the scaffold surface was further validate via exosomal protein quantification (Figure 2D).

The functionalization of MDs-NFATc1 on the PLA/Exo scaffold was confirmed via confocal laser scanning microscopy images (Figure 2E and F), which depict the spatial distribution of the functionalized MDs-NFATc1 within the scaffold matrix.

To assess the effective delivery of MDs released from the MDs-NFATc1/PLA-Exo hybrid scaffold to target cells, the internalization of MDs was examined using confocal laser scanning microscopy. As shown in Figure 2G–I, the successful internalization of FITC-labeled MDs can be noted following culture with RAW264.7 macrophages, which FITC-labeled MDs were confined to the cytoplasmic component around perinuclei areas at 6 h post-treatment. Additionally, a continuous increase of FITC-labeled MDs in RAW264.7 macrophages was found at 24 h, indicating sustained release efficiency and cellular uptake over time.

To examine the cellular internalization of MSC-Exo released from MDs-NFATc1/PLA-Exo hybrid scaffold into recipient cells, MSC-Exo were labeled with PKH67 before scaffold fabrication. As depicted in Figure 2H–J, the green fluorescence signal exhibited a substantial increase at 1 day and 3 days post-incubation in hBMSCs, suggesting effective internalization of MSC-Exo from the PLA-Exo scaffold into recipient cells. These results highlight the potential efficacy of the hybrid scaffold system in facilitating the delivery of MSC-Exo into cellular targets.

Biocompatibility Test of Different Scaffolds

The biocompatibility of various scaffolds was assessed using MTT assay and live/dead staining in macrophages. Results showed no significant differences among PLA, MDs-NFATc1/PLA, and MDs-NFATc1/PLA-Exo groups in the MTT assay from day 1 to day 3. Additionally, OD values increased markedly by day 3 compared to day 1 in all groups, indicating no cytotoxicity of the scaffolds (Figure 3A and 3B). Live/dead staining revealed predominantly viable cells after 1 and 3 days of co-culture, with increased cell density by day 3 across all groups (Figure 3C and D).

Subsequently, the biocompatibility of various scaffolds in hBMSCs at different time points was analyzed using MTT assay and live/dead staining. As depicted in Figure 3E and F, hBMSCs demonstrated significantly higher proliferation rates and viability across all groups, indicating the absence of evident toxicity from PLA, MDs-NFATc1/PLA, and MDs-NFATc1/PLA-Exo scaffolds. Live/dead staining results further illustrated green-colored viable hBMSCs co-cultured with PLA, MDs-NFATc1/PLA, and MDs-NFATc1/PLA-Exo scaffolds on both day 1 and day 3 (Figure 3G and H).

The Effect of MDs-NFATc1/PLA-Exosome Hybrid Scaffold on the Differentiation of Osteoclast Precursors

The effects of different scaffolds on osteoclast progenitor differentiation were assessed via TRAP staining. After 7 days of osteoclast differentiation, multinucleated and TRAP-positive osteoclasts were observed in all groups cultured with M-CSF and RANKL. However, incubation with MDs-NFATc1/PLA scaffold or MDs-NFATc1/PLA-Exo scaffold significantly reduced osteoclastic differentiation compared to the PLA group (Figure 4A). Quantitative analysis revealed a significant decrease in the number of TRAP-positive cells in the MDs-NFATc1/PLA scaffold or MDs-NFATc1/PLA-exosome hybrid scaffold groups (Figure 4B).

The Effect of MDs-NFATc1/PLA-Exosome Hybrid Scaffold on the Osteogenic Differentiation of hBMSCs

To assess the impact of different scaffolds on hBMSCs' osteogenic differentiation, ALP expression was examined via ALP immunofluorescent staining. Figure 5A shows a significant increase in ALP expression in the MDs-NFATc1/PLA-exosome hybrid scaffold group after 14 days of osteogenic induction compared to PLA and MDs-NFATc1/PLA groups.

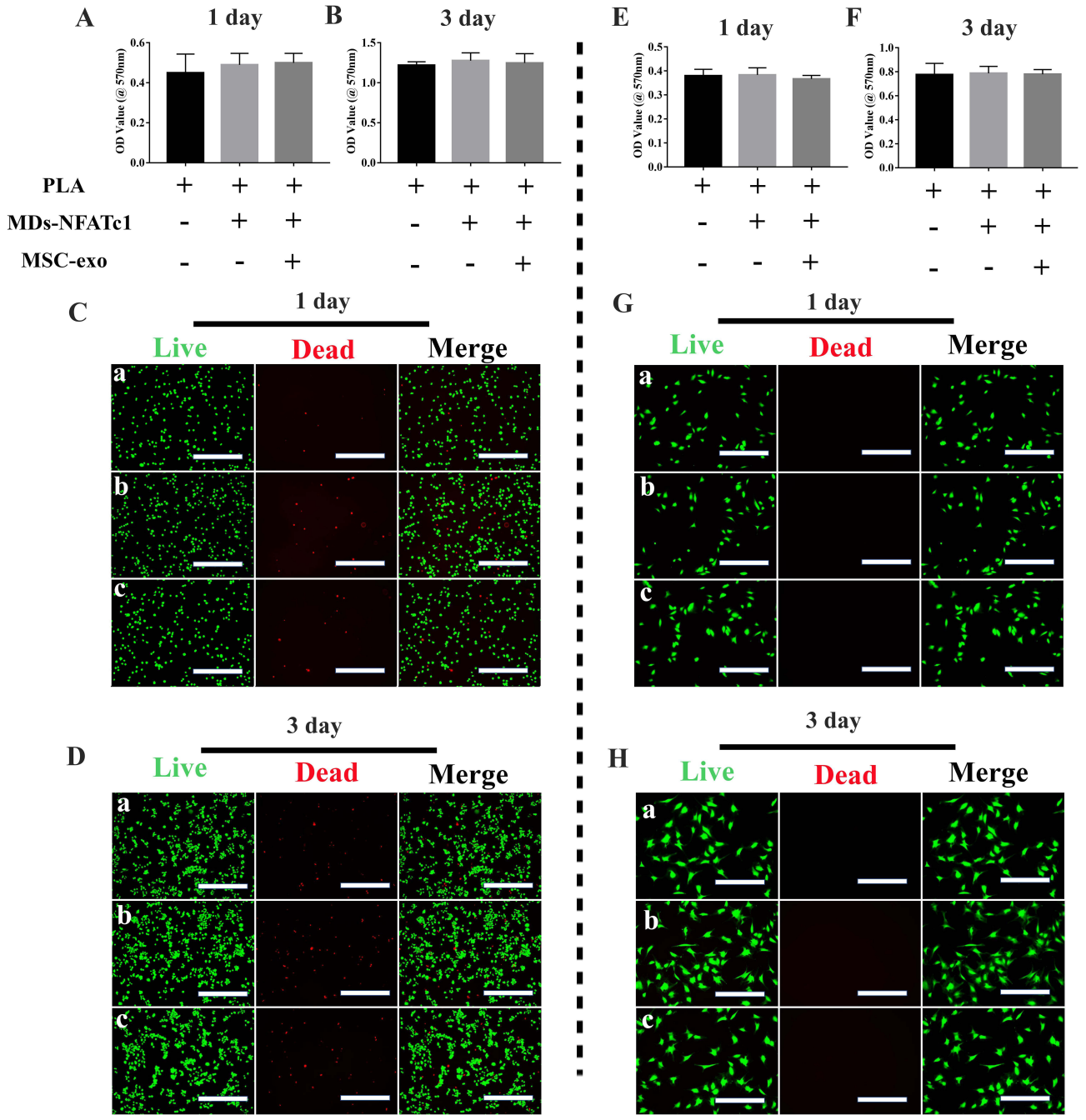

Figure 3 Biocompatibility and morphology following different scaffolds treatment. (**A** and **B**) MTT cell proliferation assay showing RAW264.7 macrophage viability following co-culture with different scaffolds. Data are shown as mean ± SD (n=3). (**C** and **D**) Representative confocal laser microscopy images of RAW 264.7 macrophages co-cultured with different scaffolds. Viable cells are indicated as green color (calcein-AM), while dead cells are labeled as red fluorescence (PI). Scale bar = 500 μm. a=PLA, b= MDs-NFATc1/PLA, and c=MDs-NFATc1/PLA-Exo. (**E** and **F**) MTT cell proliferation assay showing hBMSCs viability after co-culturing with different scaffolds. (**G** and **H**) Representative fluorescence staining images of hBMSCs co-cultured with different scaffolds. Scale bar = 500 μm.

OCN immunofluorescent staining (Figure 5B) also indicated higher OCN expression in hBMSCs cultured with MDs-NFATc1/PLA-exosome hybrid scaffold compared to PLA and MDs-NFATc1/PLA groups. However, no significant differences were observed between the PLA and MDs-NFATc1/PLA groups. Additionally, ALP staining result further revealed a highest ALP expression in the MDs-NFATc1/PLA-exosome hybrid scaffold group (Figure 5C and D).

To evaluate in vitro mineralization, alizarin red S staining was performed at 21 days to detect calcium-containing mineral deposits (Figure 5E and F). hBMSCs cultured with MDs-NFATc1/PLA-exosome hybrid scaffold exhibited

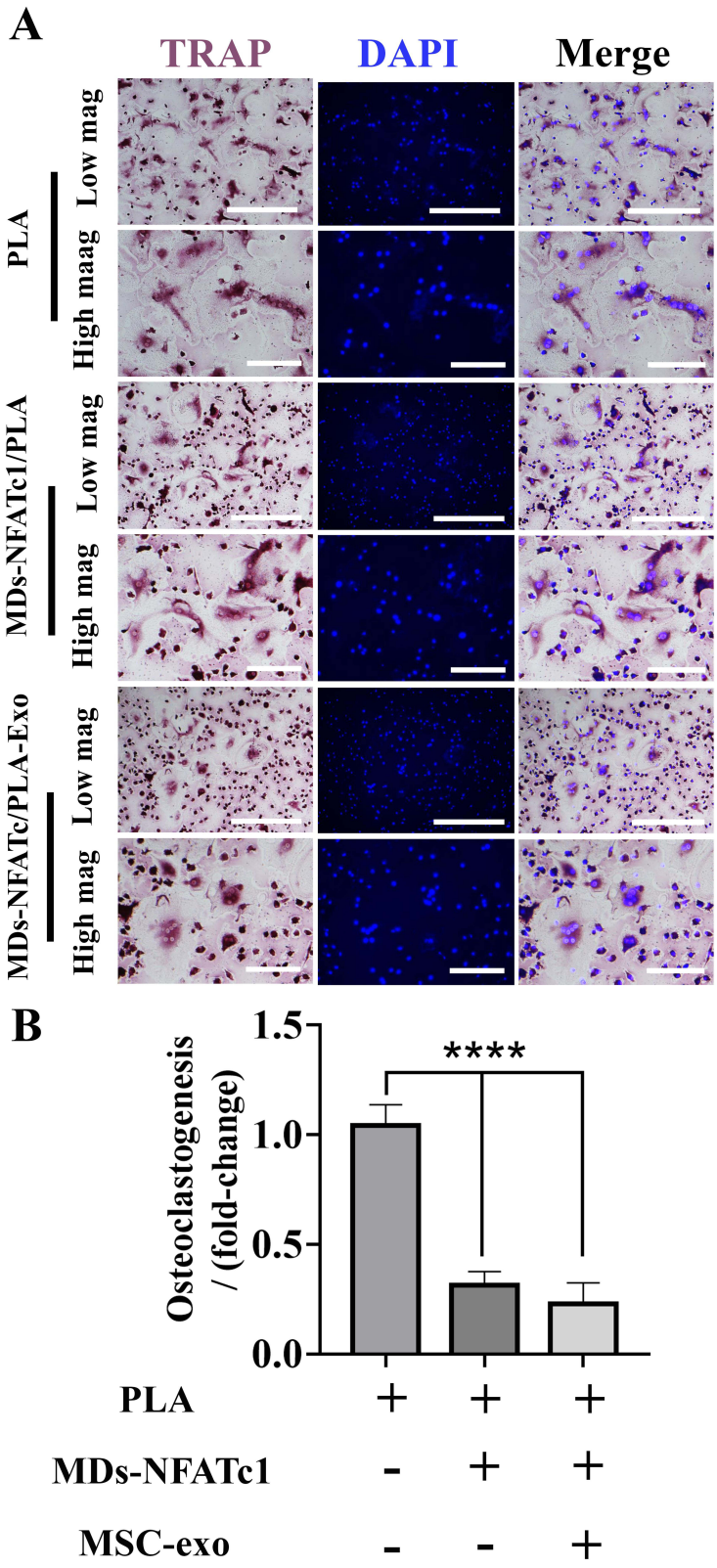

Figure 4 MDs-NFATc1/PLA and MDs-NFATc1/PLA-exosome hybrid scaffold regulates in vitro osteoclast differentiation and formation. (**A**) Representative images of TRAP-positive osteoclasts. Osteoclast precursor cells were cultured with M-CSF and RANKL in the presence of different scaffolds for 7 days, subsequently examined via TRAP staining. (**B**) The number of TRAP-positive osteoclasts were counted. Data represents the mean ± SD (n = 3). Significant difference: ****$p < 0.0001$. Scale bar=500 μm (low magnification). Scale bar=200 μm (high magnification).

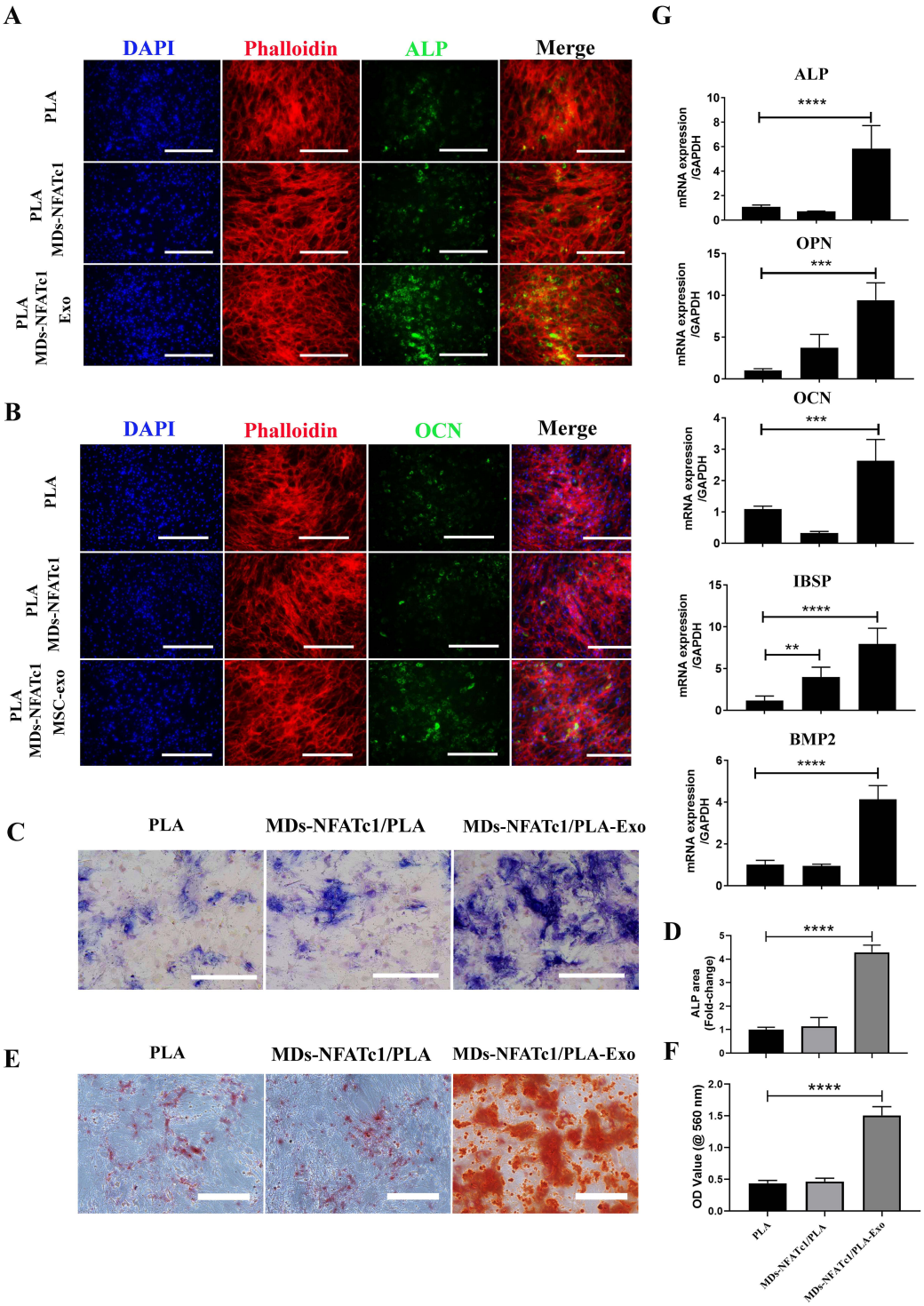

Figure 5 Effect of different scaffolds on the osteogenic differentiation potential in hBMSCs. (**A**) Immunofluorescence staining of ALP expression in hBMSCs following co-culture with different scaffolds in osteogenic differentiation medium for 14 days. Images were captured using a confocal laser scanning microscopy. Scale bar=500 μm. (**B**) Immunofluorescence staining of OCN expression in hBMSCs following co-culture with different scaffolds in osteogenic differentiation medium for 14 days. Images were captured using a confocal laser scanning microscopy. Scale bar=500 μm. (**C**) Representative ALP staining images of hBMSCs following co-culture with different scaffolds in osteogenic differentiation medium for 14 days. Scale bar=500 μm. (**D**) Quantification of ALP areas. ****$p < 0.0001$. (**E**) Representative images of alizarin red S-stained mineralized nodules at 21 days. MDs-NFATc1/PLA-exosome scaffold enhanced mineralized nodules formation compared to PLA and MDs-NFATc1/PLA scaffolds. Scale bar=200 μm. (**F**) Calcium nodules formation was eluted and measured using a microplate reader. ****$p < 0.0001$. (**G**) Gene expression levels of osteogenic-related genes in hBMSCs were assessed at 14 days. GAPDH was used as a housekeeping gene. Data represents the mean ± SD ($n = 3$). Significant difference: **$p < 0.01$, ***$p < 0.001$, ****$p < 0.0001$.

significantly higher calcium deposit formation compared to PLA and MDs-NFATc1/PLA groups, with no significant differences between PLA and MDs-NFATc1/PLA groups.

To further evaluate the osteogenic phenotype in hBMSCs, the expression of osteogenic differentiation marker genes in hBMSCs were assessed using RT-qPCR. Figure 5G demonstrates that MDs-NFATc1/PLA-exosome hybrid scaffold significantly increased the expression of osteogenesis-related markers.

The Effect of MDs-NFATc1/PLA-Exosome Hybrid Scaffold on the Cytokine Expression in hBMSCs

To explore the impact of the MDs-NFATc1/PLA-exosome hybrid scaffold on the modulation of cytokine expression in hBMSCs, cytokine array analysis was conducted. As shown in Figure 6A and B, the results indicated that supernatant from hBMSCs following MDs-NFATc1/PLA-exosome hybrid scaffold treatment showed significantly increased expression of angiogenin, endoglin, IGFBP-3, MCP-1, and SDF-1α, when compared to MDs-NFATc1/PLA scaffold.

Discussion

Current approaches used in clinical settings to accelerate bone regeneration include bone-grafting methods and the use of bone substitute materials or various pro-osteogenic factors. However, the treatment of fractures, especially osteoporotic-related fractures, and post-traumatic complications, remains a major challenge in clinical practice. From a mechanical standpoint, osteoporosis is an age-related condition marked by an imbalance in bone remodeling, involving excessive osteoclastic activity and compromised osteoblastic functions. This imbalance ultimately results in the disruption of bone microarchitecture and a decrease in bone mineral density. As a biodegradable polymer scaffold, PLA scaffolds produced by 3D printing are commonly used as bone scaffolds in tissue engineering. However, PLA scaffolds possess some major disadvantages, such as low cell adhesion and lack of bioactivity, etc. To address these limitations, we proposed a hybrid modification strategy to augment the bifunctionality of PLA scaffolds. Exosomes derived from MSCs have shown potential therapeutic effect by promoting bone regeneration. Furthermore, NFATc1 is a critical transcriptional factor to regulate osteoclastogenesis and osteoclast formation. Therefore, in this study we fabricated a hybrid PLA scaffold by incorporating microdroplets (MDs) encapsulated NFATc1-siRNA in order to regulate osteoclast overactivity and MSC-exosomes immobilized inner PLA surface in order to regulate the bone forming environment and osteogenesis. Consequently, the dual functionalized PLA scaffolds could be used as potential bioactive scaffold for bone regeneration.

Exosomes are nanoscale vesicles possess the remarkable capability to ferry vital macromolecules, such as DNA, mRNA, non-coding RNAs, microRNAs (miRNA), lipids, and proteins, from donor cells to recipient cells, thus influencing various cellular processes and physiological functions.[43] Specifically, MSC-derived exosomes are believed to play an important role in bone healing process, as compromised exosome release will lead to delayed fracture healing.[44] In recent years, scaffolds modified with MSC-Exo have shown great promise for bone regeneration. For example, Su et al fabricated exosome-functionalized polycaprolactone (PCL) fibers and investigated its immunomodulatory responses of these fibers towards tissue repair, which the release of MSC-derived exosomes from the scaffold affects the immune cells response and subsequent tissue repair outcomes in vivo.[45] Sun et al fabricated MSC-Exo modified 3D-printed silk fibroin/collagen I/nano-hydroxyapatite scaffold and then evaluated the impact of the MSC-Exo-modified scaffold on bone repair in alveolar bone defects. The results indicated that the incorporation of MSC-Exo into the scaffold enhanced the regenerative potential of the scaffold, leading to improved bone healing outcomes.[46] In this study, we focused on utilizing hBMSCs-derived exosomes to modify the pristine PLA scaffold. Initially, we isolated exosomes from hBMSCs using a previously established protocol.[47] Examination of the isolated exosomes revealed a cup-shaped morphology, consistent with findings reported in existing literature.[48,49] To label the exosomes, we employed PKH 67, a non-toxic fluorescent dye commonly utilized for this purpose.[50] Subsequent cellular uptake studies demonstrated the internalization of exosomes into RAW264.7 macrophages and hBMSCs, as indicated by the accumulation of PKH67-labeled green fluorescence puncta around peri-nuclear regions. These observations are consistent with previous research.[51,52]

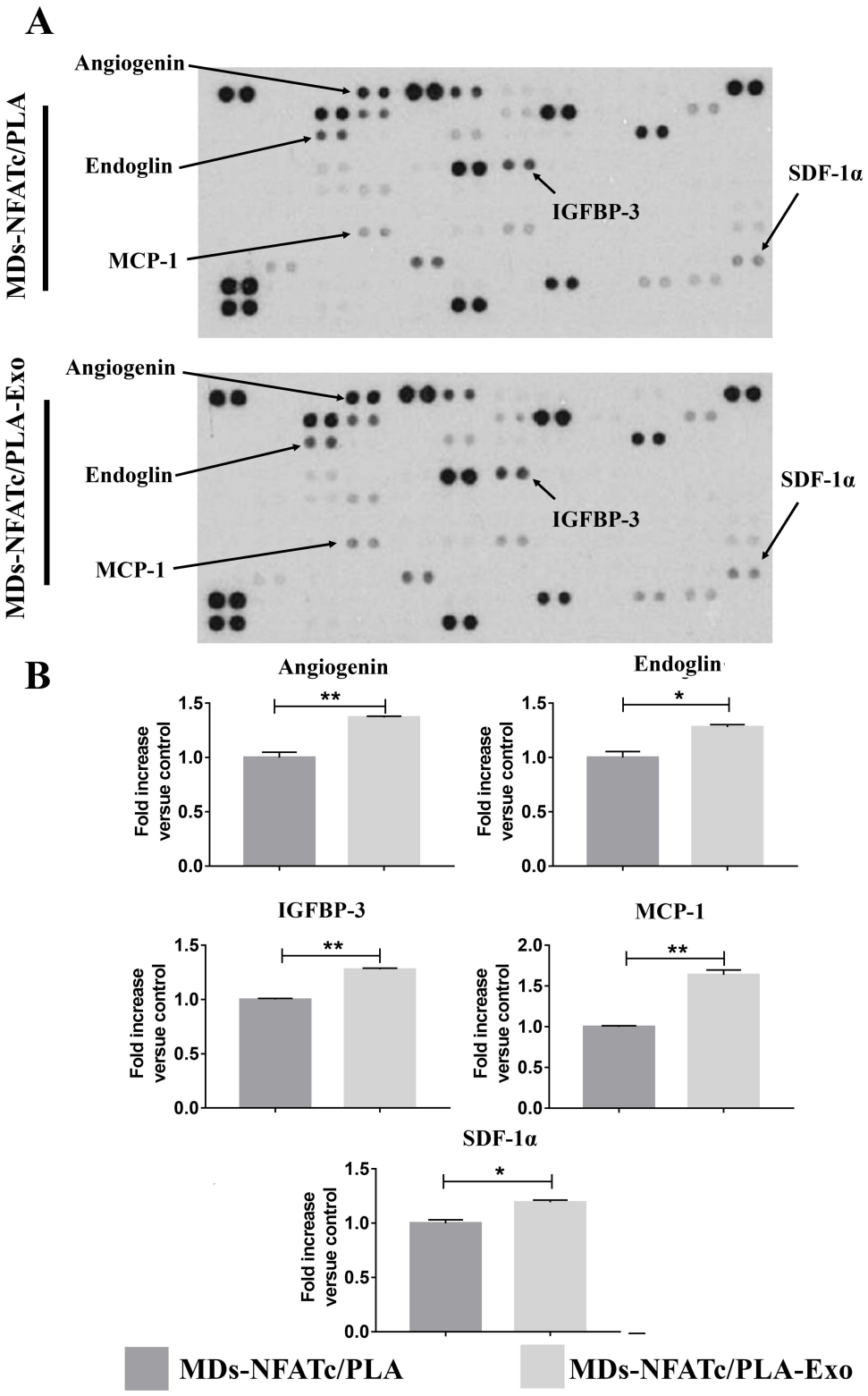

Figure 6 Cytokine and chemokine production levels following treatment with different scaffolds. (**A**) Representative images of cytokine antibody array. The Human XL Cytokine Array Kit can detect a total of 105 cytokine differences between samples. hBMSCs were co-cultured with MDs-NFATc1/PLA or MDs-NFATc1/PLA-Exo scaffold for 3 days, and the cell culture supernatant was collected for human proteome XL cytokine array. (**B**) Quantification of cytokine array assay. Significant difference: *$p < 0.05$, **$p < 0.01$. The mean signal (pixel density) of the duplicate spot pairs was measured through densitometry, with background signal subtraction and normalization using the positive control samples.

Various PLA-based scaffolds have been utilized as templates for the controlled delivery of bioactive molecules and MSCs. These scaffolds serve as a three-dimensional structure for successful cell attachment and differentiation. For example, Bahraminasab et al compared the bone regeneration potential of MSCs-loaded PLA scaffold and PLA cell-free scaffold using cranial bone defects models and found significant increased bone formation in MSCs-loaded PLA scaffold.[53] Han et al developed 3D printed PLA scaffold with the dual modification of human bone morphogenetic protein-2 (rhBMP-2) and/or MSCs. Their results showed good biocompatibility in vitro and significantly increased bone formation following dual hybrid scaffold treatment.[54] In this study, we employed a novel approach by dual targeting osteoclastogenesis and osteogenesis, respectively. The bioactive MDs-NFATc1 released from MDs-NFATc1/PLA-Exo scaffold can be clearly viewed by MDs internalization study, as evidenced by FITC-green fluorescent particles in the cytoplasm. In addition, our results confirmed the interaction between MSC-Exo and 3D printed PLA scaffold, as evidence by the confocal laser scanning microscopy imaging, which is consistent with our previous study.[38] The internalization of exosome into target cells are essential for exosomes to exert their regulatory roles.[55,56] In this study, we also observed gradual release of MSC-Exo from bioactive MDs-NFATc1/PLA-Exo hybrid scaffold, as evidenced by the presence of cytoplasmic punctate green fluorescence in hBMSCs. MSCs-derived exosomes have been demonstrated to have positive effects on cell proliferation, migration, and differentiation in diverse in vitro models.[57] In this study, we further supported that the bioactive MDs-NFATc1/PLA-Exo scaffold showed good cytocompatibility, indicating that it supported cell viability and function without causing detrimental effects. Similar to our previous study,[38] we also observed pro-osteogenic function of MDs-NFATc1/PLA-Exo hybrid scaffold as evidenced by significant increase of ALP expression, osteogenic-related marker genes expression, and mineralization.

Osteoclasts are the cells involved in bone resorption during normal bone remodeling, which are important in maintaining healthy bone turnovers.[58] In pathologic conditions (eg, osteoporosis, rheumatoid arthritis, periodontal disease, etc), however, excess osteoclastic activity was frequently recorded in a variety of pathological conditions characterized by increased bone turnover, leading to an imbalance between osteoclastic bone resorption and osteoblastic bone formation.[59] Following initiation of osteoclastogenesis by RANK and RANKL interactions, a number of down-stream intracellular signaling pathways are activated, including the recruitment of TNF receptor-associated factor (TRAF) adaptor proteins,[60] c-Fos, NF-kappaB.[61] etc. The activation of NFATc1, one of the most important transcription factors, is crucial for osteoclast differentiation and the expression of osteoclast-specific genes.[33] In this study, our results demonstrated a significant reduction in the number of osteoclasts in MDs-NFATc1/PLA-Exo hybrid scaffold group. The role of NFATc1 in the regulation of osteoclast differentiation and activity has been extensively studied. For example, Aliprantis et al investigated the effect of conditional knockout of the NFATc1 in mice resulted in osteoclast-deficient osteopetrosis.[62] The importance of NFATc1 in osteoclast differentiation is also evident in NFATc1-deficient embryonic stem cells, which fail to differentiate into osteoclasts following RANKL stimulation.[63]

The regulatory role of MDs-NFATc1/PLA-Exo hybrid scaffold was further validated by analyzing the release of soluble factors such as cytokines, chemokines, and growth factors, which could provide insights into scaffold's ability to modulate MSC behaviors. Indeed, MSCs are highly appreciated for their paracrine effects, which a variety of cytokines were secreted by MSCs, including vascular endothelial growth factor (VEGF), transforming growth factor beta (TGF-β), etc.[64] These secreted factors play critical roles in would healing and bone regeneration process.[65] Our study revealed a significant increase of angiogenin, endoglin, IGFBP-3, MCP-1, and SDF-1α following treatment with the MDs-NFATc1 /PLA-exosome hybrid scaffold. These results indicates that modulation of these important cytokines, may potentially contributing to the increased osteogenesis observed in our studies. Angiogenin is one of the most important factors for inducing angiogenesis in vivo.[66] For example, Kim et al fabricated an angiogenin-loaded bovine bone powder-based scaffold and investigated its bone regenerating ability using a rabbit calvarial bone defect model. Their results indicated the in vivo implantation of the angiogenin-loaded scaffold resulted in a significant increase of new bone and blood vessels formation.[67] In addition, endoglin plays an important role in angiogenesis and vascular remodeling processes.[68] These results suggest a potential regulatory role of our MDs-NFATc1/PLA-exosome hybrid scaffold in angiogenesis, which angiogenesis and osteogenesis are intricately interconnected and must be tightly coordinated for proper bone function in physiological conditions.[69] Therefore, further research is warranted to specifically evaluate the scaffold's effect on angiogenesis, which will further enhance our comprehension for its regulatory roles.

Conclusion

In conclusion, the bioactive MDs-NFATc1/PLA-Exo scaffold demonstrated excellent biocompatibility and was shown to significantly reduce osteoclast formation while enhancing the osteogenic differentiation of hBMSCs and modulating cytokine expression. Although the study demonstrated promising results in vitro, further investigations are necessary to validate its efficacy in vivo. Specifically, there is a need for studies to assess the safety and effectiveness of the MDs-NFATc1/PLA-Exo scaffold in osteoporotic animal models, examining its biological activity and long-term effects.

Acknowledgments

Peng Luo and Yi Zhang are co-first authors for this study.

Funding

This research received financial support from the National Natural Science Foundation of China (Grant no. 82060620 and 31960209), Outstanding Youth Scientific Fund of Guizhou Province (Grant no. Qian Ke He Platform Talents YQK[2023] 039), Guizhou Science and Technology Program Project (Grant no. Qiankehe Foundation - ZK[2023] General 502), Scientific Research Program of Guizhou Provincial Department of Education (Grant no. QJJ [2023] 019), Science and Technology Foundation of Guizhou Provincial Department of Education (Grant no. QJJ[2023]020), Zunyi Science and Technology Fund Project (Grant no. Zunyi Kehe HZ Zi [2021]40), and Future Eminent Clinician Plan of Zunyi Medical University (Grant no. 2022-02).

Disclosure

The authors declare that they have no competing interests in this work.

References

1. Lupsa BC, Insogna K. Bone health and osteoporosis. *Endocrinol Metab Clin North Am*. 2015;44(3):517–530. doi:10.1016/j.ecl.2015.05.002
2. Center JR, Bliuc D, Nguyen TV, Eisman JA. Risk of subsequent fracture after low-trauma fracture in men and women. *JAMA*. 2007;297(4):387–394. doi:10.1001/jama.297.4.387
3. Sözen T, Özışık L, Başaran N. An overview and management of osteoporosis. *Eur J Rheumatol*. 2017;4(1):46–56. doi:10.5152/eurjrheum.2016.048
4. A CM, C HN, M CE, et al. The epidemiology of osteoporosis. *Br Med Bull*. 2020;133(1):105–117. doi:10.1093/bmb/ldaa005
5. Shen Y, Huang X, Wu J, et al. The global burden of osteoporosis, low bone mass, and its related fracture in 204 countries and territories, 1990–2019. *Front Endocrinol*. 2022;13:882241. doi:10.3389/fendo.2022.882241
6. Florencio-Silva R, Sasso GR, Sasso-Cerri E, et al. Biology of bone tissue: structure, function, and factors that influence bone cells. *Biomed Res Int*. 2015;2015:421746. doi:10.1155/2015/421746
7. Dallas SL, Prideaux M, Bonewald LF. The osteocyte: an endocrine cell. and more. *Endocr Rev*. 2013;34(5):658–690. doi:10.1210/er.2012-1026
8. Aoki S, Shimizu K, Ito K. Autophagy-dependent mitochondrial function regulates osteoclast differentiation and maturation. *Biochem Biophys Res Commun*. 2020;527(4):874–880. doi:10.1016/j.bbrc.2020.04.155
9. Zhang C, Song C. Combination therapy of PTH and antiresorptive drugs on osteoporosis: a review of treatment alternatives. *Front Pharmacol*. 2020;11:607017. doi:10.3389/fphar.2020.607017
10. Hanley DA, Adachi JD, Bell A, Brown V. Denosumab: mechanism of action and clinical outcomes. *Int J Clin Pract*. 2012;66(12):1139–1146. doi:10.1111/ijcp.12022
11. Zhang J, Saag KG, Curtis JR. Long-term safety concerns of antiresorptive therapy. *Rheum Dis Clin North Am*. 2011;37(3):387–400. doi:10.1016/j.rdc.2011.08.001
12. Sterling JA, Guelcher SA. Biomaterial scaffolds for treating osteoporotic bone. *Curr Osteoporos Rep*. 2014;12(1):48–54. doi:10.1007/s11914-014-0187-2
13. Association C O. Diagnosis and treatment of osteoporotic fractures. *Orthop Surg*. 2009;1(4):251–257. doi:10.1111/j.1757-7861.2009.00047.x.
14. Chan BP, Leong KW. Scaffolding in tissue engineering: general approaches and tissue-specific considerations. *Eur Spine J*. 2008;17(Suppl 4):467–479. doi:10.1007/s00586-008-0745-3
15. Narayanan G, Vernekar VN, Kuyinu EL, Laurencin CT. Poly (lactic acid)-based biomaterials for orthopaedic regenerative engineering. *Adv Drug Deliv Rev*. 2016;107:247–276. doi:10.1016/j.addr.2016.04.015
16. C M-PMO, B BAC, N TB, et al. Biomimetic mineralization on 3D printed PLA scaffolds: on the response of human primary osteoblasts spheroids and in vivo implantation. *Polymers*. 2020;13(1). doi:10.3390/polym13010074
17. Gregor A, Filová E, Novák M, et al. Designing of PLA scaffolds for bone tissue replacement fabricated by ordinary commercial 3D printer. *J Biol Eng*. 2017;11:31. doi:10.1186/s13036-017-0074-3
18. Tai YL, Chen KC, Hsieh JT, Shen TL. Exosomes in cancer development and clinical applications. *Cancer Sci*. 2018;109(8):2364–2374. doi:10.1111/cas.13697
19. Qin J, Xu Q. Functions and application of exosomes. *Acta Pol Pharm*. 2014;71(4):537–543.
20. Yu B, Zhang X, Li X. Exosomes derived from mesenchymal stem cells. *Int J Mol Sci*. 2014;15(3):4142–4157. doi:10.3390/ijms15034142
21. S TSH, Y WJR, Sim SJY, et al. Mesenchymal stem cell exosomes in bone regenerative strategies-a systematic review of preclinical studies. *Mater Today Bio*. 2020;7:100067. doi:10.1016/j.mtbio.2020.100067

22. Liu Y, Ma Y, J ZJ, et al. Exosomes: a novel therapeutic agent for cartilage and bone tissue regeneration. *Dose Response*. 2019;17(4):1559325819892702. doi:10.1177/1559325819892702
23. Shokravi S, Borisov V, A ZB, et al. Mesenchymal stromal cells (MSCs) and their exosome in acute liver failure (ALF): a comprehensive review. *Stem Cell Res Ther*. 2022;13(1):192. doi:10.1186/s13287-022-02825-z
24. Teng X, Chen L, Chen W, et al. Mesenchymal stem cell-derived exosomes improve the microenvironment of infarcted myocardium contributing to angiogenesis and anti-inflammation. *Cell Physiol Biochem*. 2015;37(6):2415–2424. doi:10.1159/000438594
25. Birtwistle L, Chen XM, Pollock C. Mesenchymal stem cell-derived extracellular vesicles to the rescue of renal injury. *Int J Mol Sci*. 2021;22(12):6596. doi:10.3390/ijms22126596
26. Carovac A, Smajlovic F, Junuzovic DSmajlovic F, Junuzovic D. Application of ultrasound in medicine. *Acta Inform Med*. 2011;19(3):168–171. doi:10.5455/aim.2011.19.168-171
27. Cai X, Jiang Y, Lin M, et al. Ultrasound-responsive materials for drug/gene delivery. *Front Pharmacol*. 2019;10:1650. doi:10.3389/fphar.2019.01650
28. Lindner JR. Microbubbles in medical imaging: current applications and future directions. *Nat Rev Drug Discov*. 2004;3(6):527–532. doi:10.1038/nrd1417
29. M LG, D WK, J SM, et al. A novel site-targeted ultrasonic contrast agent with broad biomedical application. *Circulation*. 1996;94(12):3334–3340. doi:10.1161/01.cir.94.12.3334
30. Yin T, Wang P, Li J, et al. Ultrasound-sensitive siRNA-loaded nanobubbles formed by hetero-assembly of polymeric micelles and liposomes and their therapeutic effect in gliomas. *Biomaterials*. 2013;34(18):4532–4543. doi:10.1016/j.biomaterials.2013.02.067
31. Cao X. RANKL-RANK signaling regulates osteoblast differentiation and bone formation. *Bone Res*. 2018;6:35. doi:10.1038/s41413-018-0040-9
32. Boyce BF, Xing L. Functions of RANKL/RANK/OPG in bone modeling and remodeling. *Arch Biochem Biophys*. 2008;473(2):139–146. doi:10.1016/j.abb.2008.03.018
33. Kim JH, Kim N. Regulation of NFATc1 in osteoclast differentiation. *J Bone Metab*. 2014;21(4):233–241. doi:10.11005/jbm.2014.21.4.233
34. Park JH, Lee NK, Lee SY. Current understanding of RANK signaling in osteoclast differentiation and maturation. *Mol Cells*. 2017;40(10):706–713. doi:10.14348/molcells.2017.0225
35. Shar A, Aboutalebianaraki N, Misiti K, et al. A novel ultrasound-mediated nanodroplet-based gene delivery system for osteoporosis treatment. *Nanomedicine*. 2022;41:102530. doi:10.1016/j.nano.2022.102530
36. T LW, Yoon J, S KS, et al. Combined antitumor therapy using in situ injectable hydrogels formulated with albumin nanoparticles containing indocyanine green, chlorin e6, and perfluorocarbon in hypoxic tumors. *Pharmaceutics*. 2022;14(1). doi:10.3390/pharmaceutics14010148
37. Zhang Y, Cao J, Jian M, et al. Fabrication of interleukin-4 encapsulated bioactive microdroplets for regulating inflammation and promoting osteogenesis. *Int J Nanomed*. 2023;18:2019–2035. doi:10.2147/ijn.s397359
38. Zhang Y, Huo M, Wang Y, et al. A tailored bioactive 3D porous poly(lactic-acid)-exosome scaffold with osteo-immunomodulatory and osteogenic differentiation properties. *J Biol Eng*. 2022;16(1):22. doi:10.1186/s13036-022-00301-z
39. Chen X, Wang S, Zhang X, et al. Dual-function injectable fibrin gel incorporated with sulfated chitosan nanoparticles for rhBMP-2-induced bone regeneration. *Appl Mater Today*. 2022;26:101347. doi:10.1016/j.apmt.2021.101347
40. Wei F, J NC, S ST, et al. A novel approach for the prevention of ionizing radiation-induced bone loss using a designer multifunctional cerium oxide nanozyme. *Bioact Mater*. 2023;21:547–565. doi:10.1016/j.bioactmat.2022.09.011
41. J LD, C TH, W WS, et al. Dopaminergic effects on in vitro osteogenesis. *Bone Res*. 2015;3:15020. doi:10.1038/boneres.2015.20
42. Schmittgen TD, K J L. Analyzing real-time PCR data by the comparative C(T) method. *Nat Protoc*. 2008;3(6):1101–1108. doi:10.1038/nprot.2008.73
43. Amiri A, Bagherifar R, Ansari Dezfouli E, et al. Exosomes as bio-inspired nanocarriers for RNA delivery: preparation and applications. *J Transl Med*. 2022;20(1):125. doi:10.1186/s12967-022-03325-7
44. Furuta T, Miyaki S, Ishitobi H, et al. Mesenchymal stem cell-derived exosomes promote fracture healing in a mouse model. *Stem Cells Transl Med*. 2016;5(12):1620–1630. doi:10.5966/sctm.2015-0285
45. Su N, Hao Y, Wang F, Hou W, Chen H, Luo Y. Mesenchymal stromal exosome-functionalized scaffolds induce innate and adaptive immunomodulatory responses toward tissue repair. *Sci Adv*. 2021;7(20). doi:10.1126/sciadv.abf7207
46. Sun X, Mao Y, Liu B, et al. Mesenchymal stem cell-derived exosomes enhance 3D-printed scaffold functions and promote alveolar bone defect repair by enhancing angiogenesis. *J Pers Med*. 2023;13(2):180. doi:10.3390/jpm13020180
47. Lu H, Zhang Y, Xiong S, et al. Modulatory role of silver nanoparticles and mesenchymal stem cell-derived exosome-modified barrier membrane on macrophages and osteogenesis. *Front Chem*. 2021;9:699802. doi:10.3389/fchem.2021.699802
48. Tang Y, Zhou Y, Li HJ. Advances in mesenchymal stem cell exosomes: a review. *Stem Cell Res Ther*. 2021;12(1):71. doi:10.1186/s13287-021-02138-7
49. Wang H, Liu Y, Li J. Tail-vein injection of MSC-derived small extracellular vesicles facilitates the restoration of hippocampal neuronal morphology and function in APP / PS1 mice. *Cell Death Discov*. 2021;7(1):230. doi:10.1038/s41420-021-00620-y
50. Dominkuš P P, Stenovec M, Sitar S, et al. PKH26 labeling of extracellular vesicles: characterization and cellular internalization of contaminating PKH26 nanoparticles. *Biochim Biophys Acta Bio*. 2018;1860(6):1350–1361. doi:10.1016/j.bbamem.2018.03.013
51. Naseri Z, Oskuee RK, Jaafari MR, Forouzandeh Moghadam M. Exosome-mediated delivery of functionally active miRNA-142-3p inhibitor reduces tumorigenicity of breast cancer in vitro and in vivo. *Int J Nanomed*. 2018;13:7727–7747. doi:10.2147/ijn.s182384
52. Saeed-Zidane M, Linden L, Salilew-Wondim D, et al. Cellular and exosome mediated molecular defense mechanism in bovine granulosa cells exposed to oxidative stress. *PLoS One*. 2017;12(11):e0187569. doi:10.1371/journal.pone.0187569
53. Bahraminasab M, Talebi A, Doostmohammadi N, et al. The healing of bone defects by cell-free and stem cell-seeded 3D-printed PLA tissue-engineered scaffolds. *J Orthop Surg Res*. 2022;17(1):320. doi:10.1186/s13018-022-03213-2
54. H HS, Cha M, Z JY, et al. BMP-2 and hMSC dual delivery onto 3D printed PLA-biogel scaffold for critical-size bone defect regeneration in rabbit tibia. *Biomed Mater*. 2020;16(1):015019. doi:10.1088/1748-605X/aba879
55. Luo T, von der Ohe JHass R, Hass R. MSC-derived extracellular vesicles in tumors and therapy. *Cancers*. 2021;13(20):5212. doi:10.3390/cancers13205212

56. Lee BC, Kang I, Yu KR. Therapeutic features and updated clinical trials of mesenchymal stem cell (MSC)-derived exosomes. *J Clin Med*. 2021;10(4). doi:10.3390/jcm10040711
57. Ren S, Wang CGuo S, Guo S. Review of the role of mesenchymal stem cells and exosomes derived from mesenchymal stem cells in the treatment of orthopedic disease. *Med Sci Monit*. 2022;28:e935937. doi:10.12659/msm.935937
58. Boyce BF, Yao Z, Xing L. Osteoclasts have multiple roles in bone in addition to bone resorption. *Crit Rev Eukaryot Gene Expr*. 2009;19(3):171–180. doi:10.1615/critreveukargeneexpr.v19.i3.10
59. Troen BR. Molecular mechanisms underlying osteoclast formation and activation. *Exp Gerontol*. 2003;38(6):605–614. doi:10.1016/s0531-5565(03)00069-x
60. Kim JH, Kim N. Signaling pathways in osteoclast differentiation. *Chonnam Med J*. 2016;52(1):12–17. doi:10.4068/cmj.2016.52.1.12
61. F BB, Yamashita T, Yao Z, et al. Roles for NF-kappaB and c-Fos in osteoclasts. *J Bone Miner Metab*. 2005;23(Suppl):11–15. doi:10.1007/bf03026317
62. O AA, Ueki Y, Sulyanto R, et al. NFATc1 in mice represses osteoprotegerin during osteoclastogenesis and dissociates systemic osteopenia from inflammation in cherubism. *J Clin Invest*. 2008;118(11):3775–3789. doi:10.1172/jci35711
63. Takayanagi H, Kim S, Koga T, et al. Induction and activation of the transcription factor NFATc1 (NFAT2) integrate RANKL signaling in terminal differentiation of osteoclasts. *Dev Cell*. 2002;3(6):889–901. doi:10.1016/s1534-5807(02)00369-6
64. Kangari P, Talaei-Khozani T, Razeghian-Jahromi IRazmkhah M, Razmkhah M. Mesenchymal stem cells: amazing remedies for bone and cartilage defects. *Stem Cell Res Ther*. 2020;11(1):492. doi:10.1186/s13287-020-02001-1
65. Lin H, Chen H, Zhao X, et al. Advances in mesenchymal stem cell conditioned medium-mediated periodontal tissue regeneration. *J Transl Med*. 2021;19(1):456. doi:10.1186/s12967-021-03125-5
66. Osorio DS, Antunes A, Ramos MJ. Structural and functional implications of positive selection at the primate angiogenin gene. *BMC Evol Biol*. 2007;7:167. doi:10.1186/1471-2148-7-167
67. Kim BS, Kim JS, Yang SS, et al. Angiogenin-loaded fibrin/bone powder composite scaffold for vascularized bone regeneration. *Biomater Res*. 2015;19:18. doi:10.1186/s40824-015-0040-4
68. Tian H, Ketova T, Hardy D, et al. Endoglin mediates vascular maturation by promoting vascular smooth muscle cell migration and spreading. *Arterioscler Thromb Vasc Biol*. 2017;37(6):1115–1126. doi:10.1161/atvbaha.116.308859
69. Grosso A, G BM, Lunger A, et al. It takes two to tango: coupling of angiogenesis and osteogenesis for bone regeneration. *Front Bioeng Biotechnol*. 2017;5:68. doi:10.3389/fbioe.2017.00068